Nanoscale

Accepted Manuscript

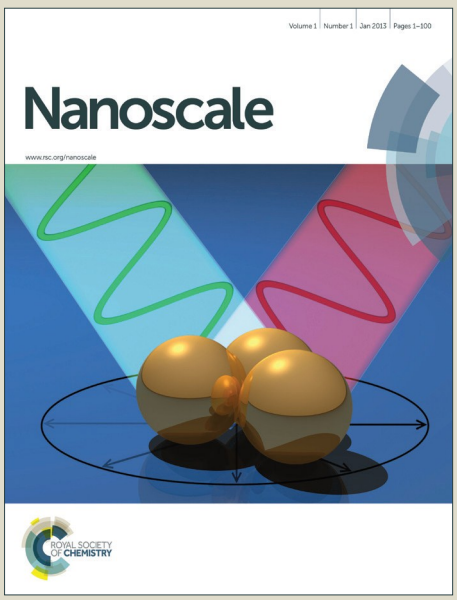

ROYAL SOCIETY OF CHEMISTRY

www.rsc.org/nanoscale

Nanoscale

ARTICLE

Ultralight Anisotropic Foams from Layered Aligned Carbon Nanotube Sheets

Received 00th January 20xx,
Accepted 00th January 20xx

DOI: 10.1039/x0xx00000x

www.rsc.org/

Shaghayegh Faraji[a], Kelly Stano[a], Ozkan Yildiz[a], Ang Li[a], Yuntian Zhu[b], and Philip D. Bradford*[a]

In this work, we present large scale, ultralight aligned carbon nanotube (CNT) structures which have densities an order of magnitude lower than CNT arrays, have tunable properties and exhibit resiliency after compression. By stacking aligned sheets of carbon nanotubes and then infiltrating with a pyrolytic carbon (PyC), resilient foam-like materials were produced that exhibited complete recovery from 90% compressive strain. With density as low as 3.8 mg/cm^3, the foam structure is over 500 times less dense than bulk graphite. Microscopy revealed that PyC coated the junctions among CNTs, and also increased CNT surface roughness. These changes in the morphology explain the transition from inelastic behavior to foam-like recovery of the layered CNT sheet structure. Mechanical and thermal properties of the foams were tuned for different applications through variation of PyC deposition duration while dynamic mechanical analysis showed no change in mechanical properties over a large temperature range. Observation of a large and linear electrical resistance change during compression of the anisotropic CNT/carbon (ACNT/C) foams makes strain/pressure sensors a relevant application. The foams have high oil absorption capacities, up to 275 times their own weight, which suggests they may be useful in water treatment and oil spill cleanup. Finally, the ACNT/C foam's high porosity, surface area and stability allow for demonstration of the foams as catalyst support structures.

1. Introduction

Fabrication of macroscopic assemblies of carbon nanotubes (CNTs) such as vertically aligned arrays [1], strands and yarns [2], aligned sheets [3], buckypapers [4] and aerogels [5], is of critical importance to understand and realize their practical applications [6]. Among those assemblies, CNT-based foams, aerogels and sponges have been studied widely due to their applications in energy absorption materials [7-9], filtration and separation [10-12], sensors [13], supercapacitors and batteries [14]. Controlling the microstructure and porosity of these foams and aerogels allows for tuning the properties to better demonstrate their potential as functional materials. This has been done by variation of the carbon source injection rate in CNT sponges fabricated though CVD [13,15] while other studies have shown tunable mechanical properties through pyrolytic carbon (PyC) infiltration for different time periods [16,17].

Despite increasing interest in porous and low-density CNT structures in recent years, there have only been a few fabrication routes for these materials. Carbon nanotube aerogels are typically created through wet-processing techniques [18-24]. Commonly, a three-dimensional network of CNTs in solution (a hydrogel) is formed first and the liquid component is further removed through critical-point-drying or freeze-drying without collapsing the preformed network structure. These methods are time-consuming and can cause agglomerations within the CNT structure. Structures typically referred to as nanotube foams and sponges are generally fabricated using a single step chemical vapor deposition (CVD) method in which, with slight modification to growth parameters such as carbon source type or catalyst treatment, either vertically aligned CNT array foams [25,26] or randomly distributed CNT sponges [27,28] can be formed. Fabrication of CNT sponge/array composite architectures using CVD has also been reported recently by Gui et al. [7-9]. In this work we demonstrate a new approach for fabrication of CNT foams by stacking aligned sheets of CNTs, drawn from spinnable nanotube arrays, and further infiltrating the stacked sheet assembly with PyC. Although the idea of dry, continuous drawing of CNTs for production of yarns, fibers and aligned sheets has been studied before[2,3,29-33], there has not been any reported CNT foam structures created by this method. CNT arrays are so far the only aligned foam structure of nanotubes reported, however, limitations in the maximum achievable CNT length of these arrays make it difficult to study their anisotropic properties. Unlike other methods, which have limitations regarding the thickness or the overall size of CNT foams, our novel fabrication process allows for synthesis of aligned CNT foam structures with any desired size, which makes it possible to measure their properties in two directions. Alignment of nanotubes resulted in anisotropic mechanical and thermal behavior of the foams, and variation in PyC coating duration allows for synthesis of ACNT/C foams with controlled microstructure, morphology and properties. Application of these CNT foams as pressure/strain sensors, thermal insulation,

a Department of Textile Engineering, Chemistry and Science, North Carolina State University, Campus Box 8301, Raleigh, NC 27695, USA

b Department of Materials Science and Engineering, North Carolina State University, Campus Box 7907, Raleigh, NC 27695, USA
** Address Correspondence to (Philip Bradford) philip_bradford@ncsu.edu*

catalyst supports and oleophilic foams for water treatment are all investigated in this work.

2. Experimental

2.1 MWCNT Synthesis

Vertically aligned CNT arrays were grown in a tube furnace via a modified version of the chlorine mediated chemical vapor deposition route [34]. The arrays were grown on a quartz substrate at 760 C and 3 Torr with acetylene as the carbon precursor and $FeCl_2$ (anhydrous 99.5% VWR) as the catalyst. The arrays were grown for 15 minutes under the flow of acetylene (600 sccm), argon (395 sccm) and chlorine (5 sccm). A detailed procedure of the growth method is explained in previous work [35].

2.2 Fabrication of the ACNT/C Foam

Aligned CNT sheets were drawn from arrays and continuously collected around two rotating parallel glass rods to make flat foam pieces. CNT winding continued until the desired sheet thickness was reached. Collecting the sheets around two small, suspended glass rods instead of a large mandrel helped the stack of aligned CNT sheets to be less compacted, resulting in a macro-porous structure. A video of the winding process is provided in the supporting information. The sheets were then separated from the glass rods using a razor and then placed inside the tube furnace for CVI of PyC. Samples were heated in tube furnace and at 800 ^{o} C in vacuum. Acetylene was then allowed to flow at 600 sccm while the pressure was maintained at 30 Torr during the desired deposition time of 60 or 120 minutes. Foam size was only limited by the CVI chamber size.

2.3 Material Characterization

Scanning electron microscopy (SEM) was conducted on a FEI XHR-Verios 460L field emission SEM (with 1 kV beam voltage and 6.3 pA beam current). All samples were used as prepared without sputtering.

Transmission electron microscopy (TEM) images were taken using a JEOL 2000FX TEM operating at 200 kV. To prepare the samples, a small piece of ACNT/C foam was dispersed in ethanol through sonication and a droplet of the dispersion was further deposited on a carbon mesh TEM grid and allowed to dry. The average diameter of pristine and PyC coated nanotubes were calculated by taking 100 measurements from TEM images for each sample using ImageJ software.

2.4 Mechanical, Electrical and Thermal Measurements

Compression testing was performed on an Instron 5544 equipped with a 100 N load cell and two flat insulating plates. Compressive load was applied either longitudinal or transverse to CNTs alignment direction. Prior to compression testing, a laser cutter (Epilog mini/helix- model 8000) was used to cut the samples into small pieces. Longitudinal samples were cut into 15 x 15 x 15 mm pieces where CNTs were aligned in thickness direction. For transverse samples, foams with dimensions of 15 x 15 x 5 mm were cut where nanotube layers were stacked in the Z direction. All samples were tested for 100 cycles from 0- 90% compressive strain at a rate of 10 mm/min.

Four-probe electrical resistance of the foams was also monitored in situ while compressing the samples. Two pieces of copper foil were used as electrodes and silver epoxy glue was applied to adhere the foam to the copper foils. Copper wires were then soldered to the copper foil electrodes.

Dynamic mechanical analysis (PerkinElmer DMA 8000) was used to measure storage modulus, loss modulus and damping ratio of the ACNT/C foams at temperature -100 to 300 C. Foams were compressed with a frequency of 1 Hz while DMA head displacement was 0.025 mm.

Room temperature thermal diffusivity was measured in both longitudinal and transverse directions by laser flash measurement technique in a Netzsch laser flash apparatus (LFA447). Longitudinal and transverse samples were cut into 12.7 x 12.7 x 2.5 mm pieces using the laser cutter. Prior to testing, a thin layer of graphite was sprayed on both sides of the samples in order to enhance the absorption of laser energy and emission of infrared (IR) radiation to the detector.

2.5 ALD of ZnO and Photodeposition Process

ALD of ZnO was performed in a custom built, hot-wall, viscous flow reactor at a temperature of 120 °C, and an operating pressure of 1 Torr. The metallorganic precursor used was diethylzinc (DEZ) (95% Strem Chemicals, Inc.), and the oxidizing agent was high purity water (Sigma Aldrich). Ultra-high purity N_2 (Machine Welders) was used as the carrier gas with a flow rate of approximately 200-300 sccm.

The ALD process began with an N_2 purge of 600 seconds followed by a DEZ dose, N_2 purge, H_2O dose, and N_2 purge. The dosing sequence was repeated for 100 cycles, after which there was a final N_2 purge for 120 seconds. The dose and purge times used in this particular study were $DEZ/N_2/H_2O/N_2$ = 0.4/30/0.2/60 sec.

Photodeposition of Ag onto ZnO-coated ACNT/C foams was conducted by first submerging samples in petri dishes containing 30 mL of a stock solution of 1e-3 M $AgNO_3$ in water. Photoreduction was carried out by exposing the petri dishes to a high-power UVA irradiation source (Intelli-Ray 400, ~ 75 mW/cm^2) for 30 minutes.

3. Results and Discussion

3.1 The ACNT/C Foam Preparation

Vertically aligned CNT arrays were grown on quartz substrate using a low pressure, chlorine mediated CVD method. The pristine CNT arrays could be easily drawn horizontally into aligned sheets (Figure 1A). Continuous collection of aligned sheets around rotating glass rods allowed for fabrication of CNT structures with any desired thickness (Figure 1B). Each wound sheet layer added approximately 30 µm to the thickness of the structure and a 9.5 x 6 x 2.5 cm piece of stacked aligned CNT sheets could be easily drawn from one CNT array (Figure 1C). As-drawn aligned CNT structures were not elastic and were permanently deformed after compression. The stack of aligned CNT sheets was then infiltrated with PyC for the desired deposition time of 60 or 120 minutes. These samples are referred to as 60-C and 120-C, respectively. Interestingly, the structural and

morphological changes after PyC infiltration made them resilient, exhibiting shape recovery after compression. As a result, ACNT/C foams could be compressed into a pellet and almost fully recover from deformations as large as 90% after removal of the external stress. This type of coating has also been found to similarly increase the elasticity of CNT aerogels [36].

This fabrication method is highly unique in that, unlike most other routes, the size of the foams is not limited. Side by side drawing of a number of arrays into aligned sheet allows for fabrication of wider pieces, while placing the rotating glass rods further from each other increases the length of the final piece. Thickness of the foams is controlled by adjusting the duration of drawing process. Density of as-drawn stacked CNT sheets was 1.6 mg/cm^3, but increased to 3.8 and 9.2 mg/cm^3 after 60 and 120 minutes of PyC infiltration, respectively. This increase in density corresponds to volume fraction rise from 0.0008 to 0.0019 and 0.0046, yielding porosity >99%.

3.2 Effects of Morphological Changes on Resiliency of ACNT/C Foams

Figure 2 shows SEM and TEM images of as-drawn CNTs and ACNT/C foams. The highly porous structure allows for gas infiltration into the CNT network and uniform PyC coating throughout the stacked sheet thickness was observed. The core-shell structure of PyC coated nanotubes is clear in Figure 2C & E where the cross section of the coated nanotubes is shown. Measurements from TEM images showed that CNT diameters increased, on average from 31 nm to 78 nm and 148 nm after 60 and 120 minutes PyC coating, respectively.

Comparing TEM images of samples 60-C and 120-C revealed that the deposited PyC becomes more disordered as the coating increases in thickness. This was also reported in previous studies of PyC coated CNTs [37-39]. A recent study of pristine and PyC coated CNT sheets [38] showed that increasing PyC coating duration increases the average ratio of disordered to graphitic carbon (I_D/I_G), as evidenced from Raman microscopy analysis. This indicates that infiltrating CNT sheets with PyC increases the structural disorder and imperfections.

Perhaps the most apparent change to the structure after PyC deposition was an increase in CNTs surface roughness. Bradford et al. [16] related this increase in surface roughness to the improved elasticity of CNT arrays after carbon deposition. When compressing an as-drawn CNT structure, the van der Waals interactions among smooth walls of nanotubes at points of contact is substantial. Thus, the structure will remain permanently deformed even after the compressive load is removed. If the surface roughness of the CNTs increases through chemical vapor infiltration (CVI) of PyC, van der Waals interactions among nanotubes decreases, allowing for separation of CNTs inside the foam and recovery of the structure as the compressive load is removed. Another structural change that can contribute to the resiliency of CNT sheets after carbon infiltration is the formation of PyC coated CNT junctions. As shown in SEM images, CNTs in as-drawn sheets are mostly aligned in spinning direction with some points of contact (bundles) between nanotubes in the same or neighboring layers. During CVI post treatment, deposited PyC layers coat these CNT junctions, increasing tube-tube integrity, which resulted in greater structural stability under compression.

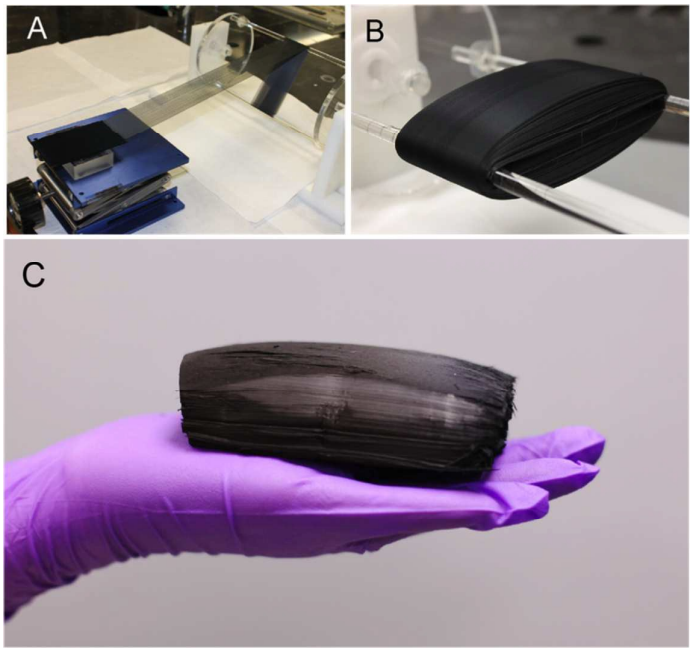

Figure 1. A) Drawing and winding of ACNT sheet. B) A thick, multi-layer ACNT sheet before separation from the glass rods. C) A large ACNT/C foam after infiltration with PyC.

In other words, *physical cross-links*, in the form of PyC coated junctions, are introduced into the structure through carbon infiltration to freeze-in or reinforce the original sheet state.

3.3 Mechanical Behaviour

Anisotropic CNT/C foams can be compressed in transverse or longitudinal directions, yielding significantly different mechanical behavior. Mechanical properties of ACNT/C foams could also be tuned for specific applications through varying PyC coating duration. Foams with shorter PyC deposition were compressed more easily than samples with longer PyC infiltration. All samples were tested for 100 cycles at 90% strain.

This strain range covers the initial linear region and also shows the plateau and the strain hardening behavior. Figure 3 shows compressive loading-unloading curves for ACNT/C foams with different PyC treatment durations tested in two directions. When compressed in the transverse direction, 60-C foam exhibited a stress of 2.4 kPa at 80% strain. The higher density foam, made with 120 minutes of PyC infiltration, showed more than a 3-fold increase in strength at the same 80% strain. Both foams showed complete shape and structural recovery from the applied stress. During subsequent compression cycles, slow accumulation of permanent compressive deformation resulted in 4.4% and 5.4% residual strain for 60-C and 120-C foams, respectively.

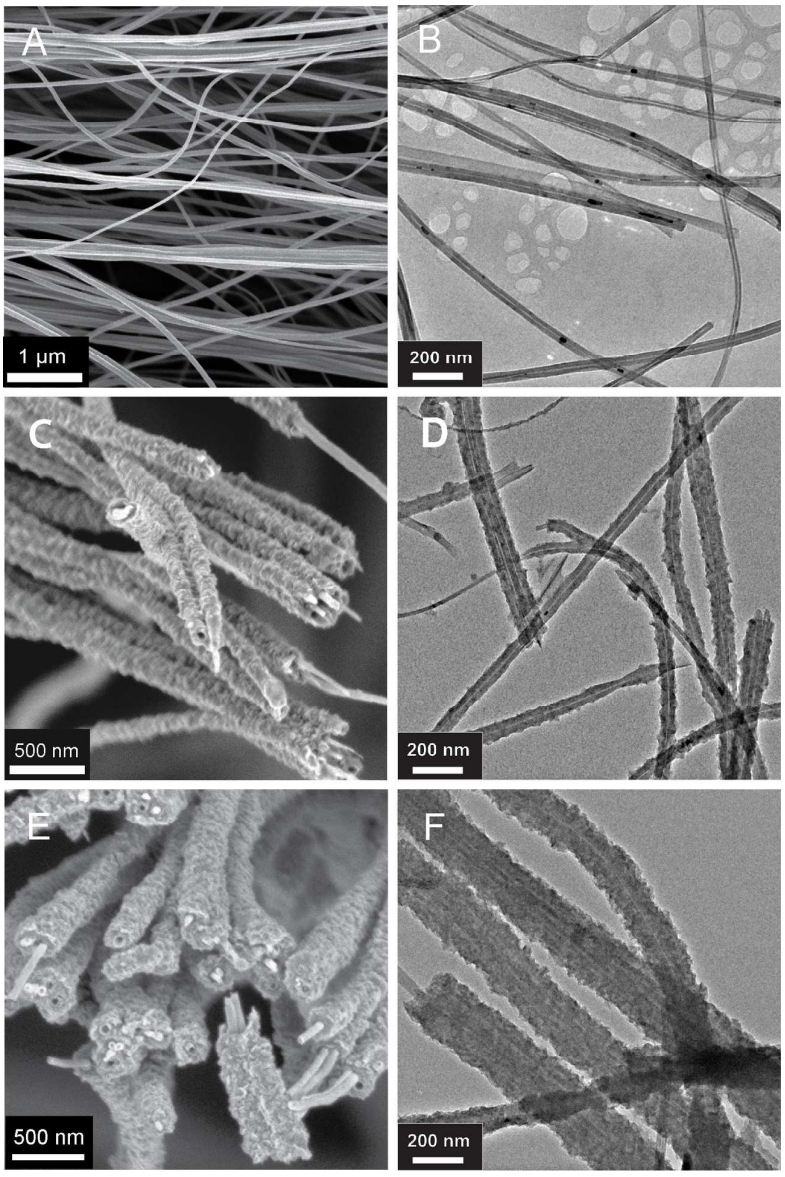

Figure 2. SEM (left) and TEM (right) characterization of samples. A,B) As-spun CNT sheets. C,D) 60-C foam and E,F) 120-C foam.

The ACNT/C foams exhibited different mechanical properties when samples were tested parallel to nanotube alignment direction. On the first cycle, compressive strength of both 60-C and 120-C foams at 80% strain was approximately three times greater. For all the samples, further densification of nanotube structure at strain values above 80% resulted in a rapid increase of the modulus.

When the longitudinal structures were compressed, energy absorption and associated energy dissipation (area of the hysteresis loops) were much greater than transversely compressed samples. The energy absorption also increased with increased PyC coating duration.

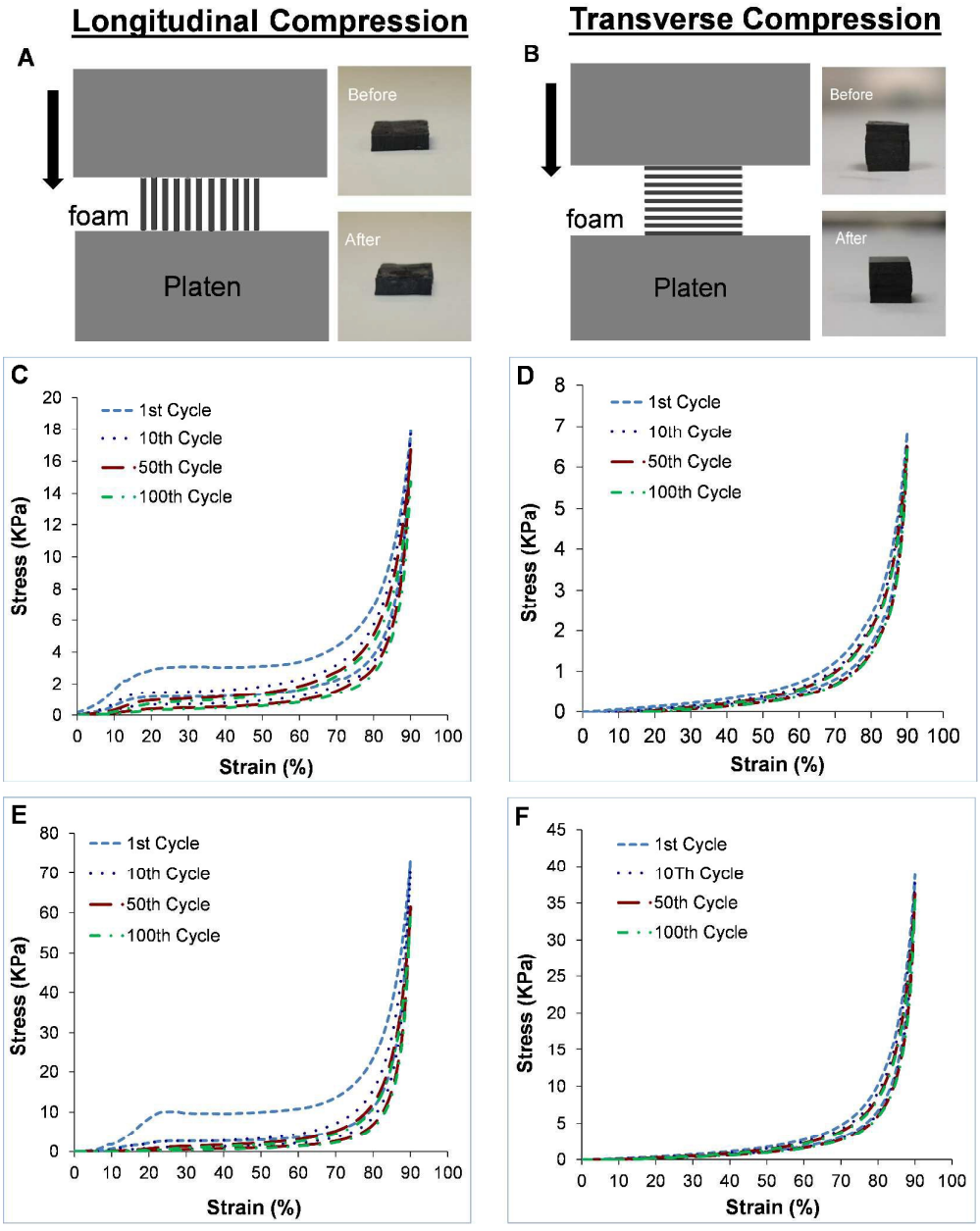

Figure 3. Compression behavior of ACNT/C foams. Schematic illustration of the samples for longitudinal (A) and transverse (B) compression testing with photographs showing foams before and after 100 cycles of compression. Compression loading-unloading curves of 60-C foam (C,D) and 120-C foam (E,F) tested in both directions.

As shown in Figure 3A, energy absorption of the foams compressed longitudinally increased and reached about 1150 kJ/m^3 after 120 minutes of PyC infiltration. This is three times greater than the energy absorption of the same foam and more than 14 times greater than that of 60-C foam when they were compressed in the transverse direction. The 120-C foam dissipated 626 kJ/m^3 energy in the initial compression cycle when compressed in longitudinal direction, which is 25% greater than that of recently reported CNT aerogels [24].

Significant hysteresis loops for the longitudinal samples during compression testing provided energy loss coefficients (dissipated energy divided by absorbed energy) of 0.47 and 0.54 in the first cycle for 60-C and 120-C foam, respectively. This is comparable to those of integrated random-aligned carbon nanotube layers (0.64) [9], carbon nanotube sponges (0.68) [8] and molecularly intercalated nano-flakes (0.55) [40]. Energy loss coefficients of both samples decreased to ~ 0.40 and was nearly constant after ten cycles.

The observed mechanical behavior (strengthening of the ACNT/C foam by increasing PyC infiltration duration) can be attributed to increased diameter of the nanotubes and also improved stability between CNTs at points of junction. Radial growth of nanotubes through depositing PyC layers increases the critical load required for bending them. While this factor is more important when compressing ACNT/C foams longitudinal to CNT alignment direction, coating nanotube junctions with PyC improves the compression strength in both directions.

Dynamic mechanical analysis (DMA) was used to further study the elastic properties of ACNT/C foams. Storage modulus, loss modulus and damping ratio of the foams were stable over a large temperature range of -100 to 300 ^{o}C. This stability is particularly useful in extreme temperature conditions where traditional polymeric foams are subject to thermal transitions, which dramatically change the mechanical properties. While the DMA instrument capability was limited to 300 ^{o}C, previous studies on PyC coated CNTs showed that these structures are stable up to 600 ^{o}C before degradation starts [38].

Storage modulus of the ACNT/C foam increased by one order of magnitude when PyC infiltration duration increased from 60 minutes to 120 minutes. No data was collected for the foams in transverse direction due to limitation of the load cell in the DMA. Figure 4B shows the DMA results for longitudinally compressed 120-C foam.

3.4 Thermal Properties

Thermal diffusivity of ACNT/C foams was measured both longitudinal and transverse to nanotube alignment direction. Longitudinal diffusivity of 60-C foam was ~ 40 mm^2/s when measured at room temperature and pressure. This value is comparable to measured diffusivity of CNT arrays and bundles [41-44], but is twice that of the CNT/C composite reported by Gong et al. [45] and is more than 10 times greater than diffusivity of nanoporous CNT sponge [46]. Increasing PyC coating duration to 120 minutes decreased the diffusivity of the foam by nearly half. It is known that phonons and vibrations of the crystal lattice play a dominant role in thermal transport of carbon materials. Interactions between phonons and structural imperfections decrease the phonon mean free path and increase their scattering [47]. Therefore, it is expected that 120-C, having a more disordered structure, would exhibit lower diffusivity. The anisotropic ACNT/C foams exhibited much lower thermal diffusivity in transverse direction: ~ 4 and 9 mm^2/s for 60-C and 120-C samples, respectively.

Thermal conductivity of ACNT/C foams was estimated from thermal diffusivity (α), specific heat (C_p), and density (ρ) and by using the equation $\lambda = \alpha \times \rho \times C_p$. Specific heat capacity of CNTs is reported to be very close to that of graphite at temperatures below 300 ^{o}K [48]. Assuming that C_p of PyC coated CNTs is equal to that of pure nanotubes, the specific heat of graphite at the corresponding temperature (710 J kg^{-1}K^{-1}) was used for PyC coated CNTs in the calculations. The thermal conductivity of 60-C and 120-C foams in longitudinal direction was calculated as 0.107 and 0.133 Wm^{-1}K^{-1}, respectively.

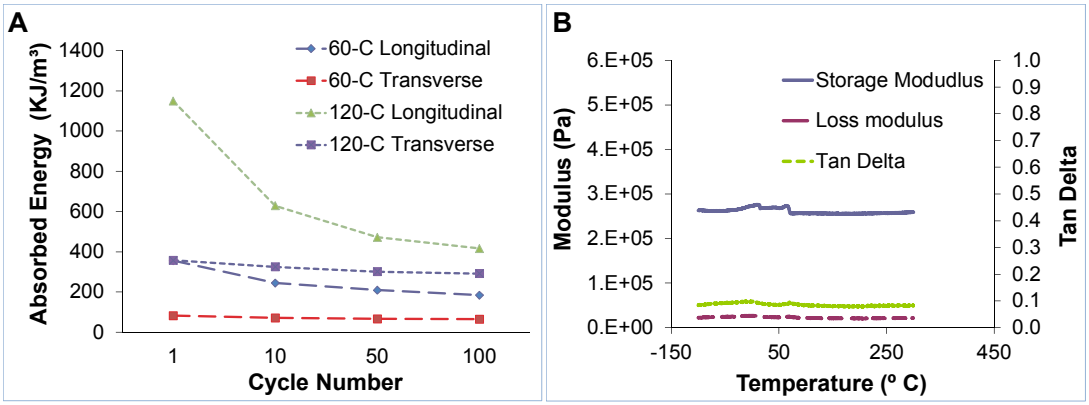

Figure 4. A) Energy absorption of ACNT/C at increasing cycle number. B) DMA data for 120-C foam tested longitudinally.

Due to much lower diffusivity of foams in transverse direction, the estimated thermal conductivities were an order of magnitude lower in that direction and were calculated to be only 0.026 and 0.027 $Wm^{-1}K^{-1}$ for 60-C and 120-C samples, respectively. The super-low thermal conductivities of ACNT/C foams is due to their extremely low densities, as well as their low thermal diffusivities (especially in transverse direction). This thermal conductivity is much lower compared to other CNT macrostructures [46, 49-51]. In fact, it is close to the lower limit of thermal conductivities of commercial thermal insulation materials (0.02-0.07 $Wm^{-1}K^{-1}$). The combination of super-low thermal conductivity of ACNT/C foams along with their high temperature stability, could lead to their use as improved insulation for high temperature applications.

It is known that high temperature heat treatments help to remove structural defects and improve crystalline quality in carbon materials [52, 53]. Raman spectroscopy studies on the graphitic structure of similar PyC coated CNT sheets have shown that the average I_D/I_G of the samples decrease after high temperature heat treatment [38]. Also, increase in lattice stack size or crystallite size (L_c) after high temperature annealing have been reported previously [38, 45]. To study the effect of annealing on thermal conductivity of ACNT/C foams, samples were heat treated in a high temperature furnace (RED DEVIL vacuum furnace WEBB 124) at 2150 °C for five hours in an argon atmosphere. Results showed that after thermal annealing, longitudinal diffusivity of 60-C and 120-C along the nanotube axis increased to 105 and 60 mm^2/s, respectively. This indicates that high temperature heat treatment enhanced the micro-crystallite size and graphitic quality of ACNT/C foams, resulting in fewer scattering centers for phonon propagation and greater thermal diffusivity. Improvement in diffusivity after heat treatment was smaller in transverse direction compared to that of longitudinal direction. This was expected since the low diffusivity of ACNT/C foams in transverse direction was mainly due to limited heat diffusion through the air, which separates the CNT layers. After high temperature annealing the foams became more anisotropic with a 10x difference in the thermal conductivity between longitudinal and transverse directions.

Figure 5 summarizes the thermal diffusivity of 60-C and 120-C foams in both directions, before and after high temperature heat treatment.

3.5 Strain/Pressure Sensors

Application of electrically conductive and compressible carbonaceous materials as pressure or strain sensors has been demonstrated previously [13, 21, 22, 26, 54-57]. Here, the dependence of electrical resistance of the foams to applied pressure was investigated *in situ* as the ACNT/C foams were compressed up to ~ 90% in both directions. A schematic of the setup for the *in situ* measurement of electrical resistance during compression is shown in Figure 6. The starting resistance of the 60-C foam for transverse configuration with no load was 10.7 Ω. Under applied compressive loading, compaction of the adjacent CNT sheet layers caused the normalized electrical resistance (R/R_0) to decrease linearly and dramatically, until reaching about 15% of the initial value. Following unloading of the compressive force, complete recovery of the electrical resistance was observed. This behavior was consistent over 100 cycles of loading and unloading (Figure 6C). 120-C foam had a lower starting electrical resistance of 8.2 Ω and showed a similar resistance change behavior upon cyclic transverse compression.

Longitudinal compression of the foams showed non-linear and less dramatic changes in resistance (Figure 6D & F). This is because in the longitudinal direction, electrons are mainly travelling along the length of nanotubes and thus, resistance of the foams is less sensitive to developing contact points between CNTs during compression. In comparison, electron transfer in the transverse direction almost completely depends on CNT-CNT contact points and resistance is more sensitive to applied compression. Another reason is the distinct behavior of the foams in longitudinal compression compared to transverse. Under transverse loading, nanotubes exhibit uniform compressibility *as an ensemble* and *collective* densification of them leads to linear change in normalized resistance. However, under longitudinal compression, CNTs are bent in a random fashion. Our results showed that the normalized resistance of the 60-C foam changed only 30 %, up to 75% strain.

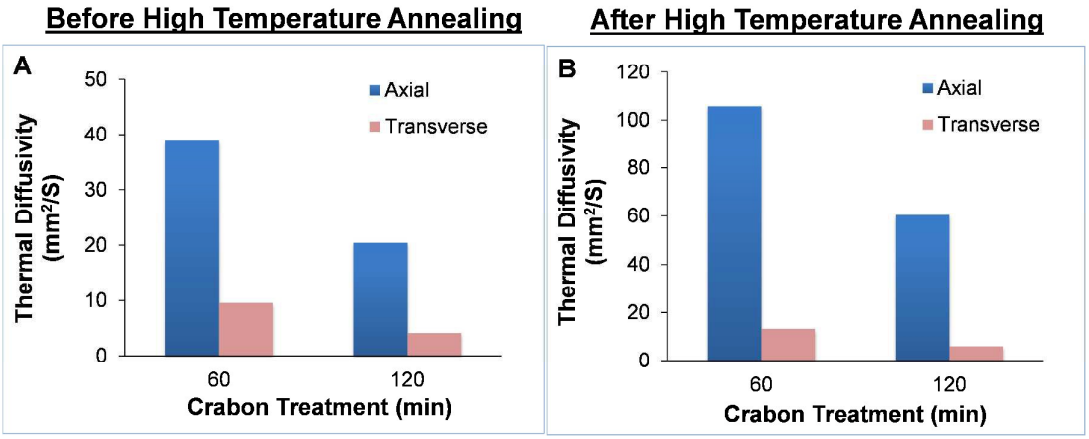

Figure 5. Thermal diffusivity of ACNT/C foams in transverse and longitudinal direction before (A) and after (B) high temperature heat treatment

After that, a faster decrease in resistance occurs at higher strain values (> 75%), where CNT foams are compressed enough that more contact points are formed between CNTs. This causes a non-linear change in normalized resistance for samples compressed in the longitudinal direction. The combination of excellent compressive recovery and high electrical sensitivity to compression, make ACNT/C foams a great candidate for large displacement strain/pressure sensors.

Given their high surface area as well as good chemical and physical stability, ACNT/C foams are excellent catalyst support materials. Zinc oxide, a technologically important wide band gap semiconductor with photocatalytic properties, was conformally deposited onto the ACNT/C foams using atomic layer deposition (ALD).

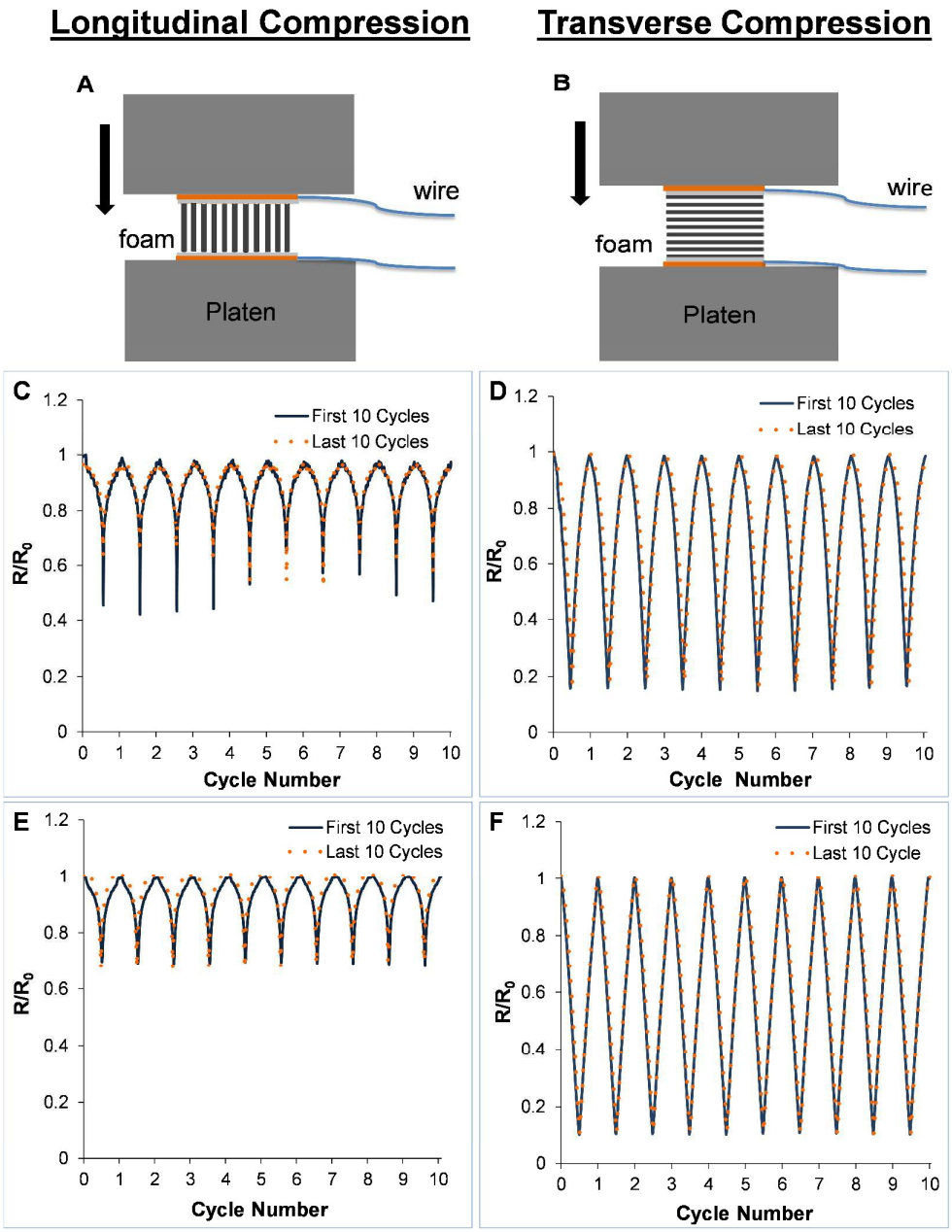

Figure 6. Illustration of sample setup for two-probe electrical resistance measured in-situ for A) longitudinal and B) transverse compression. Changes in electrical resistance for 60-C foam (C,D) and 120-C foam (E,F) tested in two directions.

3.

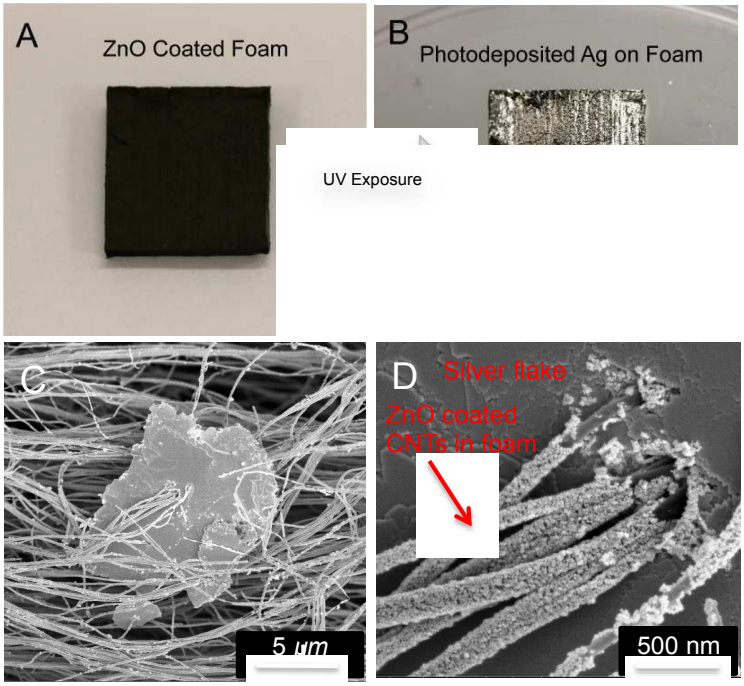

Figure 7. Application of ACNT/C foams as catalyst support materials. A,B) Photograph of ZnO coated foam before and after photodeposition of Ag. C,D) SEM image of photodeposited Ag on ACNT/C foam.

To demonstrate the catalytic behaviour of the ZnO-ACNT/C hybrid, photoreduction of Ag was carried out by submerging the samples in a dilute aqueous solution of $AgNO_3$ and placing them under a UV lamp. After 30 minutes of UV exposure, an obvious color change from black to silver indicated a dense coating of Ag. This was also verified in SEM images provided in Figure 7. As is seen in Figure 7C, silver was photoreduced and deposited at the surface of the foams in form of random flakes. A higher magnification SEM image in Figure 7D shows the rough surfaces of the ZnO coated ACNT/C foam. The background of the image is the deposited silver flake.

These images show that while the ALD ZnO layer forms a conformal coating on every carbon coated nanotube, silver is deposited as flakes on the surface of the foams. Foams without the ZnO coating did not remove any silver from solution. Photodeposition of Ag on the surface of ACNT/C foams demonstrates the ability to use these foams as low density catalyst support materials that are dimensionally stable when submerged in liquids.

3.7 Selective Liquid Absorption

ACNT/C foams are highly hydrophobic with contact angle of ~150^o but posses high absorption capacities for organic solvents and oils.

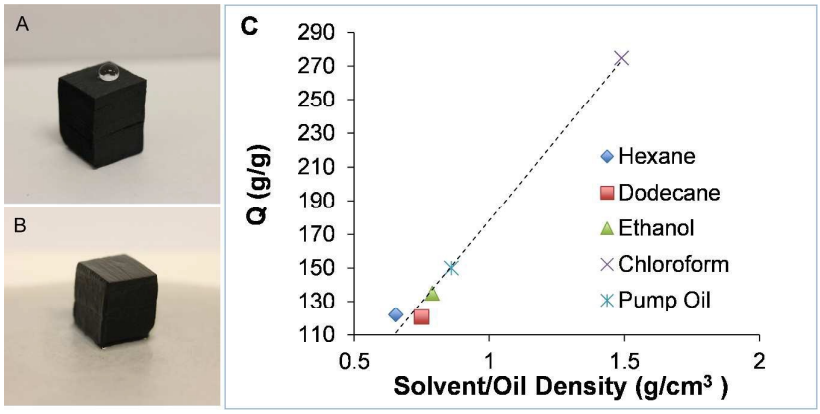

Figure 8. A,B) Photographs showing hydrophobic (A) and oleophilic (B) nature of ACNT/C foams. C) Absorption capacity (Q) of ACNT/C foams measured for a range of organic solvents and oils in terms of their density. The dashed line shows increasing absorption capacity for higher density liquids.

The surface energy difference between the foam and the liquids creates this difference in wetting behaviour. The ACNT/C foams are highly porous and do not support wetting of high surface energy liquids like water. However, non-polar liquids typically have a very low surface energy and so they readily wet the foam surface and absorb into the structure. Absorption capacities, Q (the ratio of the final weight after full absorption to the initial weight of the foam), for a 60-C foam are presented in Figure 8. The foams demonstrated high absorption capacities for various organic solvents and oils, achieving 120-275 g g^{-1} depending on the liquid density.

After liquid absorption, the foams could be recycled by desorption of the liquid sorbent by heat. To do this, the sorbent was first partially removed by squeezing the foam using a hot aluminium block. The foam was then left on the hot block which led to evaporation of the remaining liquid by heat. After liquid removal, the foams retained their original shape and size. A video of the desorption process for recycling of the foams is provided in the supporting information. Compressive mechanical properties of the foams were measured after five cycles of liquid absorption and desorption. The compressive mechanical properties of the recycled foam showed almost no change in compressive strength at 80% strain after the liquid absorption and desorption cycles.

Conclusions

In summary, stacked dry-spun sheets of aligned CNTs were infiltrated with PyC through a CVI method to fabricate anisotropic carbon nanotube foams with ultralow densities. Unlike other routes for fabrication of CNT aerogels, foam and sponges, this processing method allows the fast synthesis of CNT foams with any desired size. Deposition of PyC made the surface of CNTs rough and coated the junctions between nanotubes inside the inter-connected network of the sheet, which led to foam-like recovery of the structure after compression. The ACNT/C foams can be tuned by changing the carbon infiltration time to control thermal transport and mechanical properties. Samples with longer PyC treatment times exhibited greater compressive strength and energy absorption while having lower thermal diffusivity. Super-low thermal conductivities (as low as 0.026 $Wm^{-1}K^{-1}$) paired with the known thermal stability of carbon materials, suggests the application of these foams as thermal insulation for high temperature applications. Also, compressive mechanical properties of ACNT/C foams were unchanged over the large temperature range of -100 to 300 ^{o} C as revealed by DMA testing. Electrical resistance of these foams showed stable, linear dependency to applied compressive strain, making these foams acceptable for application as strain/pressure sensors. Oleophilic ACNT/C foams showed great oil absorption capacity, up to 275 times their own weight, making them applicable for water treatment and oil spill cleanup while photoreduction experiments demonstrate the potential of these foams to be used as catalyst support materials.

Acknowledgements

This work was supported by Air Force Office of Scientific Research grant no. FA9550-12-1-0088. The authors acknowledge the use of the Analytical Instrumentation Facility (AIF) at North Carolina State University, which is supported by the State of North Carolina and the National Science Foundation. The authors thank Prof. Russell Gorga for use of the Instron and Prof. Jesse Jur for time on the ALD equipment.

References

1 K. Hata, D. N. Futaba, K. Mizuno, T. Namai, M. Yumura and S. Iijima, *Science*, 2004, **306**, 1362-1364.

2 M. Zhang, K. R. Atkinson and R. H. Baughman, *Science*, 2004, **306**, 1358-1361.

3 M. Zhang, S. Fang, A. A. Zakhidov, S. B. Lee, A. E. Aliev, C. D. Williams, K. R. Atkinson and R. H. Baughman, *Science*, 2005, **309**, 1215-1219.

4 M. Endo, H. Muramatsu, T. Hayashi, Y. Kim, M. Terrones and M. Dresselhaus, *Nature*, 2005, **433**, 476-476.

5 M. B. Bryning, D. E. Milkie, M. F. Islam, L. A. Hough, J. M. Kikkawa and A. G. Yodh, *Adv Mater*, 2007, **19**, 661-664.

6 L. Liu, W. Ma and Z. Zhang, *Small*, 2011, **7**, 1504-1520.

7 Z. Zeng, X. Gui, Z. Lin, L. Zhang, Y. Jia, A. Cao, Y. Zhu, R. Xiang, T. Wu and Z. Tang, *Adv Mater*, 2013, **25**, 1185-1191.

8 X. Gui, Z. Zeng, Y. Zhu, H. Li, Z. Lin, Q. Gan, R. Xiang, A. Cao and Z. Tang, *Adv Mater*, 2014, **26**, 1248-1253.

9 Z. Zeng, X. Gui, Q. Gan, Z. Lin, Y. Zhu, W. Zhang, R. Xiang, A. Cao and Z. Tang, *Nanoscale*, 2014, **6**, 1748-1755.

10 X. Gui, Z. Zeng, Z. Lin, Q. Gan, R. Xiang, Y. Zhu, A. Cao and Z. Tang, *ACS applied materials & interfaces*, 2013, **5**, 5845-5850.

11 H. Li, X. Gui, L. Zhang, S. Wang, C. Ji, J. Wei, K. Wang, H. Zhu, D. Wu and A. Cao, *Chemical Communications*, 2010, **46**, 7966-7968.

12 H. Li, X. Gui, L. Zhang, C. Ji, Y. Zhang, P. Sun, J. Wei, K. Wang, H. Zhu and D. Wu, *Advanced Functional Materials*, 2011, **21**, 3439-3445.

13 X. Gui, A. Cao, J. Wei, H. Li, Y. Jia, Z. Li, L. Fan, K. Wang, H. Zhu and D. Wu, *ACS nano*, 2010, **4**, 2320-2326.

14 D. N. Futaba, K. Hata, T. Yamada, T. Hiraoka, Y. Hayamizu, Y. Kakudate, O. Tanaike, H. Hatori, M. Yumura and S. Iijima, *Nature materials*, 2006**, 5**, 987-994.

15 X. Gui, Z. Lin, Z. Zeng, K. Wang, D. Wu and Z. Tang, *Nanotechnology,* 2013, **24**, 0857050-85705-7.

16 P. D. Bradford, X. Wang, H. Zhao and Y. Zhu, *Carbon,* 2011, **49**, 2834-2841.

17 W. Zhao, Y. Li, S. Wang, X. He, Y. Shang, Q. Peng, C. Wang, S. Du, X. Gui and Y. Yang, *Carbon*, 2014, **76**, 19-26.

18 M. B. Bryning, D. E. Milkie, M. F. Islam, L. A. Hough, J. M. Kikkawa and A. G. Yodh, *Adv Mater*, 2007, **19**, 661-664.

19 L. Camilli, C. Pisani, E. Gautron, M. Scarselli, P. Castrucci, F. D'Orazio, M. Passacantando, D. Moscone and M. De Crescenzi, *Nanotechnology*, 2014, **25**, 065701.

20 A. Cao, P. L. Dickrell, W. G. Sawyer, M. N. Ghasemi-Nejhad and P. M. Ajayan, Science, 2005, 310, 1307-1310 R. R. Kohlmeyer, M. Lor, J. Deng, H. Liu and J. Chen, *Carbon*, 2011, **49**, 2352-2361.

21 H. Sun, Z. Xu and C. Gao, Adv Mater, 2013, 25, 2554-2560.

22 J. Zou, J. Liu, A. S. Karakoti, A. Kumar, D. Joung, Q. Li, S. I. Khondaker, S. Seal and L. Zhai, *Acs Nano*, 2010, **4**, 7293-7302.

23 S. Nardecchia, D. Carriazo, M. L. Ferrer, M. C. Gutiérrez and F. del Monte, *Chem. Soc. Rev.,* 2013, **42**, 794-830.

24 M. Karakaya, D. Saini, R. Podila, M. J. Skove, A. M. Rao, R. Thevamaran and C. Daraio, *Advanced Engineering Materials,* 2014 .

25 A. Cao, P. L. Dickrell, W. G. Sawyer, M. N. Ghasemi-Nejhad and P. M. Ajayan, *Science*, 2005, **310**, 1307-1310.

26 J. Suhr, P. Victor, L. Ci, S. Sreekala, X. Zhang, O. Nalamasu and P. Ajayan, Nature *nanotechnology*, 2007, **2**, 417-421..

27 X. Gui, J. Wei, K. Wang, A. Cao, H. Zhu, Y. Jia, Q. Shu and D. Wu, *Adv Mater,* 2010, **22**, 617-621.

28 X. Gui, A. Cao, J. Wei, H. Li, Y. Jia, Z. Li, L. Fan, K. Wang, H. Zhu and D. Wu, *ACS nano,* 2010, **4**, 2320-2326.

29 C. Jayasinghe, S. Chakrabarti, M. J. Schulz and V. Shanov, *J. Mater. Res.,* 2011, **26**, 645-651.

30 M. B. Jakubinek, M. B. Johnson, M. A. White, C. Jayasinghe, G. Li, W. Cho, M. J. Schulz and V. Shanov, *Carbon,* 2012, **50**, 244-248.

31 N. Behabtu, C. C. Young, D. E. Tsentalovich, O. Kleinerman, X. Wang, A. W. Ma, E. A. Bengio, R. F. ter Waarbeek, J. J. de Jong, R. E. Hoogerwerf, S. B. Fairchild, J. B. Ferguson, B. Maruyama, J. Kono, Y. Talmon, Y. Cohen, M. J. Otto and M. Pasquali, *Science,* 2013, **339**, 182-186.

32 N. Behabtu, M. J. Green and M. Pasquali, *Nano Today,* 2008, **3**, 24-34.

33 A. E. Aliev, J. Oh, M. E. Kozlov, A. A. Kuznetsov, S. Fang, A. F. Fonseca, R. Ovalle, M. D. Lima, M. H. Haque, Y. N. Gartstein, M. Zhang, A. A. Zakhidov and R. H. Baughman, *Science,* 2009, **323**, 1575-1578.

34 Y. Inoue, K. Kakihata, Y. Hirono, T. Horie, A. Ishida and H. Mimura, *Appl. Phys. Lett.,* 2008, **92**, 213113-213113-3.

35 O. Yildiz and P. D. Bradford, *Carbon,* 2013, **64**, 295-304.

36 K. H. Kim, Y. Oh and M. Islam, *Nature nanotechnology,* 2012, **7**, 562-566.

37 J. Yuguang, Y. Zhang, Q. Zhang, Z. Rufan, P. Li, W. Qian and F. Wei, *Nanoscale,* 2013, **5**, 6181-6186 .

38 S. Faraji, K. Stano, C. Rost, J. Maria, Y. Zhu and P. D. Bradford, *Carbon,* 2014, **79**, 113-122 .

39 G. Zheng, H. Sano and Y. Uchiyama, *Carbon,* 2013, **57**, 267-273.

40 C. Yu, Z. Chen, H. Li, J. Turner, X. C. Zeng, Z. Jin, J. Jiang, B. Youssef and L. Tan, *Adv Mater,* 2010, **22**, 4457-4461.

41 X. Huang, J. Wang, G. Eres and X. Wang, *Carbon,* 2011, **49**, 1680-1691.

42 W. Lin, J. Shang, W. Gu and C. Wong, *Carbon,* 2012, **50**, 1591-1603.

43 T. Borca-Tasciuc, S. Vafaei, D. Borca-Tasciuc, B. Wei, R. Vajtai and P. Ajayan, *J. Appl. Phys.,* 2005, **98**, 054309-054309-6.

44 J. Hou, X. Wang, C. Liu and H. Cheng, *Appl. Phys. Lett.,* 2006, **88**, 181910-181910-3.

45 Q. Gong, Z. Li, X. Bai, D. Li, Y. Zhao and J. Liang, *Materials Science and Engineering: A,* 2004, **384**, 209-214.

46 J. Chen, X. Gui, Z. Wang, Z. Li, R. Xiang, K. Wang, D. Wu, X. Xia, Y. Zhou and Q. Wang, *ACS applied materials & interfaces,* 2011, **4**, 81-86.

47 A. M. Marconnet, M. A. Panzer and K. E. Goodson, *Reviews of Modern Physics*, 2013, **85**, 1295-1327.

48 C. Masarapu, L. Henry and B. Wei, *Nanotechnology,* 2005, **16**, 1490-1494.

49 M. E. Itkis, F. Borondics, A. Yu and R. C. Haddon, *Nano letters,* 2007, **7**, 900-904.

50 M. B. Jakubinek, M. A. White, G. Li, C. Jayasinghe, W. Cho, M. J. Schulz and V. Shanov, *Carbon,* 2010, **48**, 3947-3952.

51 A. E. Aliev, M. H. Lima, E. M. Silverman and R. H. Baughman, *Nanotechnology,* 2010, **21**, 035709-035709-11.

52 K. Behler, S. Osswald, H. Ye, S. Dimovski and Y. Gogotsi, *Journal of Nanoparticle Research,* 2006, **8**, 615-625.

53 Q. Gong, Z. Li, Y. Wang, B. Wu, Z. Zhang and J. Liang, *Mater. Res. Bull.,* 2007, **42**, 474-481.

54 J. Li, J. Li, H. Meng, S. Xie, B. Zhang, L. Li, H. Ma, J. Zhang and M. Yu, *Journal of Materials Chemistry A,* 2014, **2**, 2934-2941.

55 V. L. Pushparaj, L. Ci, S. Sreekala, A. Kumar, S. Kesapragada, D. Gall, O. Nalamasu, A. M. Pulickel and J. Suhr, *Appl. Phys. Lett.,* 2007, **91**, 153116-153116-3.

56 A. Lu, G. Hao and Q. Sun, *Angewandte Chemie International Edition,* 2013, **52**, 7930-7932.

57 L. Camilli, C. Pisani, M. Passacantando, V. Grossi, M. Scarselli, P. Castrucci and M. De Crescenzi, *Appl. Phys. Lett.,* 2013, **102**, 183117-183117-3.